Role of particle size of mesoporous zeolite y on its catalytic cracking behaviors in 1,3,5-triisopropylbenzene

J. Zhao[a], L. Q. Yang[a], L. Yu[a], X. M. Zhao[c], Y. C. Hao[a], Z. J. Zhao[a,b,*]
[a]*School of Chemistry and Chemical Engineering, Xingtai University, No. 88 Quanbei East Street, Qiaodong District, Xingtai 054001, China*
[b]*Hebei Functional Polymer Materials Research and Engineering Application Technology Innovation Center, Xingtai University, No. 88 Quanbei East Street, Qiaodong District, Xingtai 054001, China*
[c]*College of Environmental Engineering, North China Institute of Science and Technology, Lang Fang 065201, China*

Different-sized mesoporous zeolites Y were synthesized using two step chemical post treatment. The catalysts were prepared and characterized by XRD, SEM, TEM, N_2 adsorption-desorption, and NH_3-TPD. The results revealed that catalyst prepared from S-MZY having average particle sizes of 200-300 nm, had a large mesopore volume (0.428 cm^3g^{-1}) and higher hierarchy factor (0.149), with a slightly drop of acidic sites amount. These catalysts were evaluated by catalytic cracking performance of TIPB. Higher mesoporousity structure of S-MCY promoted the addition of TIPB conversion (2.49 %) and yield of DIPB (6.33 %). Meanwhile, less acid sites reduced the deep cracking of DIPB, leding to a decreasion of cumene. Then, it can be concluded that the small crystal size has a profound effect on the catalytic performance of mesoporous zeolite.

(Received January 15, 2021; Accepted April 25, 2021)

Keywords: Zeolite Y, Mesoporous, Post treatment, Particle size, Surfactants-assisted

1. Introduction

Zeolite molecular sieves are crystalline microporous aluminosilicates, which are wildly used in different applications such as adsorption process, acid-catalyzed reactions and ion exchange etc [1-3]. Meanwhile, the micropore system also limits the transformation property of reactant and product molecules in/out of zeolites. To overcome the above problems, considerable efforts are focused on the introduction of mesopores systems in zeolites materials [4]. Hierarchical zeolites Y, which is one of the most important zeolites in the chemical industry, have promoted remarkable improvement in catalytic cracking of heavy oil and selectivity of light oil.

Depending on the previous reports, the introduced wider pores within hierarchical zeolites Y can be grouped into intra- and intercrystalline voids [5]. So far, mainly two methods, i.e. chemical post-treatment and templating synthesis strategy, are used to obtain intracrystalline mesopores. Templating synthesis strategy is usually based on adding mesopore templating agent during the process of crystallization to induce formation of mesopores. But there are some problems such as high cost, low accessibility, so it is difficult to popularize in the catalysis industry [6, 7]. Alternatively, another approach is chemical post-treatment, using acid or base etching to removal framework aluminium (dealumination) or silicon species (desilication) [4, 8]. And Intercrystalline mesopores are produced by damages of zeolitic structures and mass loss [9, 10]. In view of the drawbacks of the common demetallation of zeolite frameworks, surfactants-assisted alkaline treatments are considered to be novel preparation methodologies, also known as post-treatments which are considered to be the promising routes to introduce mesoporosities into zeolites [11-13]. Using this method, mesostructures can be introduced with the zeolite microporosities well preserved. Comparing with the native microporous zeolites, a series of material properties changes are shown in micrometer sized zeolites, such as, the larger

* Corresponding author: zjqz925@163.com

intercrystalline space, the increased external surfacearea, and more exposed pore mouths [14]. Shao et al [15] synthesized four ZSM-5 zeolites with different crystal sizes, and found that the external surface area of the zeolites decreased with crystal crystal size increase, and the acid density firstly increased. So, the application of nanozeolites in the catalytic reactions can shorten diffusion path and improve catalytic activity [16-18], as well as increase the stability of reaction medium.

It has been proved that surface area and porosity are important characteristics of catalysts [19, 20]. The crystal size of zeolites has a great influence on the catalytic performance [21]. In order to obtain highly active mesoporous zeolite Y, it is critical to identify the crystal size effect of mesoporous zeolite Y. In this work, different-sized mesoporous zeolites Y were synthesized using two step chemical post-treatment, which firstly lactic acid leaching and then surfactants-assisted alkaline treatments in the presence of hexadecyltrimethyl ammonium bromide (CTAB) to prepare mesoporous zeolite Y. And effect of the crystal size on its 1,3,5-triisopropylbenzene(TIPB) catalytic performance was investigated and studied. Meanwhile, the tailored mesoporosity effects on the textural and acidic properties were evaluated.

2. Experimental

Zeolite Y was prepared using common hydrothermal method according to the literature [5]. The precursor solution with zeolite Y was prepared by sodium metaaluminate (95 wt%, Beijing GuoHua Chemical Material Co.), sodium hydroxide (96 wt%, Beijing Chemical Reagents Company), water glass (28.0 wt% SiO_2, Lanzhou Petro Chemical Co., Petro China Company Ltd.), and deionized water. The initial aluminosilicate gel of the reaction mixture was (2-2.5)Na_2O: 1Al_2O_3: (6.0-8.0)SiO_2: 150H_2O. Different-sized crystals were synthesized through regulating the aging time of directing agent. The precursor gel was transferred to a stainless steel autoclave and hydrothermally treated for a period of time. The obtained samples repeatedly ion-exchanged three times with 0.1 mol/L $(NH_4)_2$ SO_4 aqueous solution. And then they were dried 393 K in air flow for 12 h. The final zeolite was denoted HZY or S-HZY, S represented small crystal size.

Mesoporous zeolites Y were prepared using a two-step method as reports [22] . First step: 1.0 g of (S-)HZY zeolite was dispersed into 10 ml of 0.1 mol/L citric acid aqueous solution with stirring at room temperature for 2 h. Then the resultant mixture was transferred into a stainless steel autoclave, and heated at 373 K for 1 h. Following this, the obtained product was filtrated and washed in deionized water and then dried. Second step: 1.0 g NH_3•2H_2O(25 wt.%) was added into 20 mL of water containing 0.48 g of CTAB with stirring. 1.0 g above-prepared zeolite was added into the mixed solution with keeping stirring for another 1 h under room temperature. After that, the mixture was transferred into a stainless steel autoclave, and heated at 423 K for 24 h. The resultant sample was filtrated, washed, dried and calcined in air at 550 °C for 4 h to get mesoporous zeolite Y, and denoted as (S-) MZY. (S-) MZY was crushed and sieved to 40–60 mesh to get mesoporous catalyst Y, which was defined as (S-) MCY.

X-ray diffraction (XRD) patterns of the prepared zeolites were recorded on a Bruker AXSD8 Advance X-ray diffractometer using nickel-filtered Cu Ka X-ray radiation at 40 kV and 30 mA. The 2θ range was scanned from 15° to 35° with a scanning rate of 2°/min.The specific surface areas and pore volumes of the zeolites were measured using a Bilder KuboX1000 system at liquid nitrogen temperature. The total specific surface areas were calculated using the Brunauer−Emmett−Teller (BET) equation. The total pore volumes were calculated from the amounts of nitrogen adsorbed at $P/P_0 = 0.98$. The micropore volumes were calculated by the t-plot method. Barrett–Joyner–Halenda (BJH) model were used to obtain pore size distribution from the desorption branches of the isotherms. Scanning electron microscopy (SEM) was used to describe the morphology of the samples on a SU8010 (Hitachi, Japan) apparatus. Transmission electron microscopy (TEM) was used to evaluate the existence of the mesostructure by a JEOL JEM-2100 electron microscope operating at 200 kV.The IR spectra analyses (FT-IR) of the zeolites were performed on a Gangdong FTIR-850 infrared spectrophotometer (Gangdong Sci. &Tech. Development Co., Ltd., China) with a resolution of 1cm^{-1}. The samples were mixed with KBr (spectroscopy grade).Temperature-programmed ammonia desorption (NH_3-TPD) of the samples

was studied on a TPD/TPR 5079 analyzer. The previously heated samples were exposed to ammonia for 15 min to ensure adsorption saturation. After removing weakly adsorbed ammonia by injecting pure nitrogen at 373 K for 1 h, the NH_3-TPD profile was recorded from 373 to 873 K at a heating rate of 10 $Kmin^{-1}$.

The catalytic cracking testing of the catalysts was determined with TIPB as the probe molecules. The catalyst (50 mg) was loaded in a tubule reactor with an inner diameter of 6 mm and the reaction was carried out at 523 K. The equipment combined with a gas chromatography by the pulse method. 1 μL of TIPB was instantaneously injected by a glass syringe through a septum at the top of the reactor, followed by continuous purging with nitrogen flow of 100 mL min -1 .The composition analyses of the reaction products were carried out on-line with a SP-3420 gas chromatography (GC) equipped with a flame ionization detector (FID). In every cracking experiment, three pulses were used and the reproducibility of the results was excellent. Catalytic activity is expressed in terms of TIPB % conversion, which is defined as follows:

$$\% \text{ TIPB conversion} = (Xi-Xf)/Xi * 100$$

$$\% \text{ selectivity} = Xd/\text{TIPB conversion}$$

where Xi is the initial feed mass fraction, Xf is the final mass fraction. Xd is mass fraction of individual product. All the percentages mentioned in the results are % until.

3. Results and discussion

X-ray diffraction (XRD) patterns illustrated in Fig.1 are typically representing the diffraction peaks of a typical topological structure of the FAU type zeolite[23]. The MZY samples showed eight characteristic diffraction peaks according to the (331), (333), (440), (533), (642), (660),(555), and (664) planes reflections of zeolite Y on the basis of SH/T 0340-92. The intensity and sharpness of peaks suggested that a good retaining of framework structure of mesoporous zeolite after acid−alkaline treating.

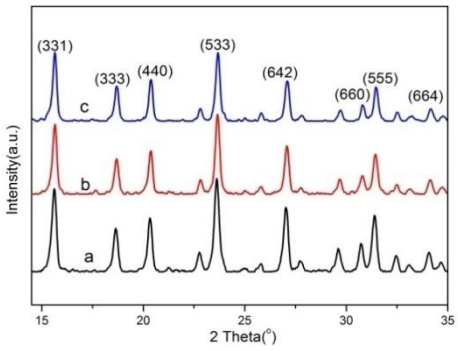

Fig. 1 XRD patterns of zeolites (a) NaY, (b) S-MZY, (c) MZY.

Fig. 2 gives the FT-IR spectra of zeolites. The curves were collected in the region of 500–4000 cm -1 to characterize the framework vibrations of zeolites. The band at 1640 cm -1 belonged to the scissor vibration arising from the proton vibration in the water molecule. The bands at 706cm-1 represented the symmetric stretching vibrations corresponding to the inner TO4 structure (T = Si, Al), respectively, whereas the bands at 788 cm-1 represented the asymmetric and symmetric stretching vibrations corresponding to the external TO4 structure (T = Si, Al), respectively. The band at 576 cm -1 was attributed to the double ring external linkage peak associated with the FAU structure, which was present in the MZY and S-MZY curves indicating

the existence of FAU framework [24]. The peaks in the range of 1300–1500 cm-1 ascribed to C–H bending vibrations can be observed only in the spectra of sample MZY and S-MZY, which were caused by hexadecyltrimethyl ammonium ions CTA+ moieties occluded in the samples[22] with using assisted reagent CTAB.

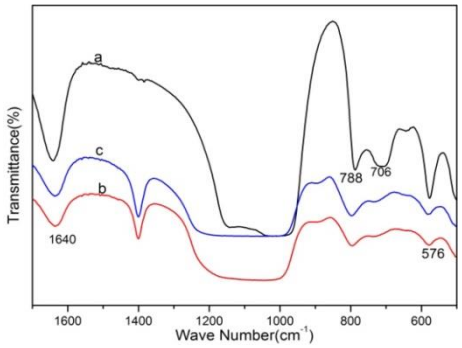

Fig. 2 FTIR spectra of zeolites (a) NaY, (b) S-MZY, (c) MZY.

The crystallite size and morphology of the zeolite samples were investigated by SEM (Fig. 3a,b). The SEM images of sample S-MZY (Fig. 3a) and MZY (Fig. 3b) showed the typical octahedral morphology consisting particle of size in the range of 200-300 nm and 700-800 nm. In addition, a few amorphous materials were observed in the samples S-MZY and MZY indicating the partial collapse of framework in the post treatment process. Furthermore, the intracrystalline mesopores inside the crystals can be observed evidently (Fig. 3c,d). The TEM images of S-MZY (Fig. 3c) showed that the single crystal exhibited more bright spots comparing to sample MZY. These bright spots were attributed to the presence of mesopores, which were likely to penetrate into crystals. The TEM images proved that small crystal size was beneficial to creating mesoporous systems.

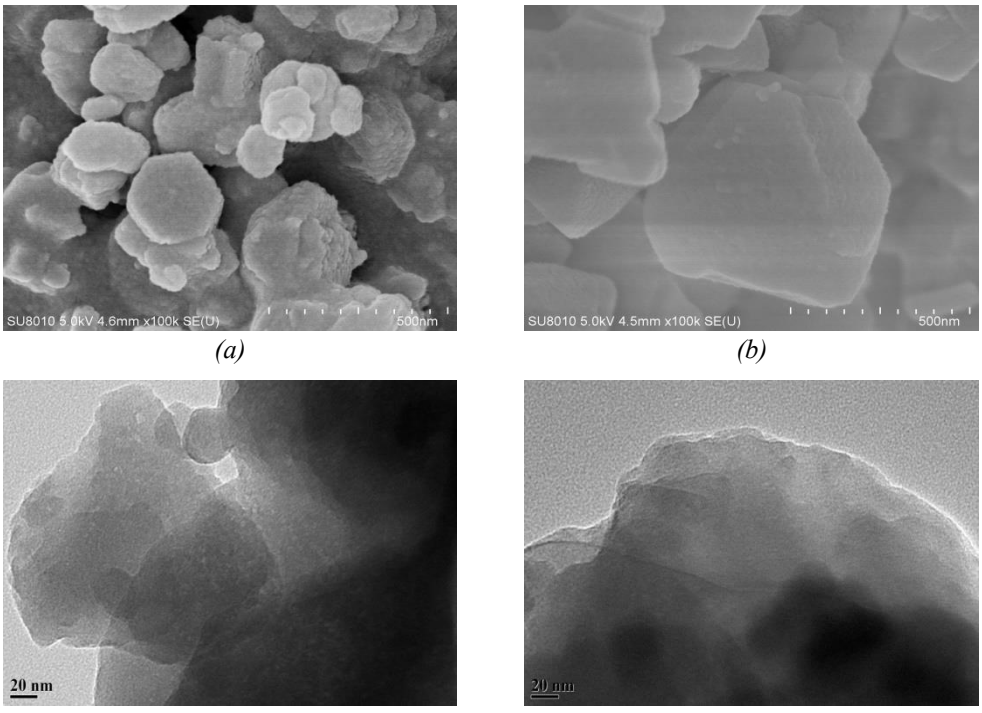

(a) *(b)*

(c) *(d)*

Fig. 3. SEM and TEM images of (a,c) S-MZY and (b,d) MZY.

Nitrogen adsorption-desorption analysis was used to evaluate textural properties of S-MCY and MCY samples. As shown in figure, S-MCY and MCY exhibitd typical type-H4 hysteresis loop (Fig. 4), which indicated the existence of textural mesopores. Whereas, the isotherm of S-MCY exhibited a more increase at relative pressure P/P_0 of 0.55-1.00, referring to MSY. The Type-H4 hysteresis loop was usually associated with slit-like pore and particles with internal gaps [25]. It indicated that higher mesopores content belonged to S-MCY, compared to MSY. BJH model is used to show the mesopore size distribution. According to observations in Fig. 5, it can be seen that pore size concentrating around 3-5 nm had been detected both in the S-MCY and MCY samples. Table 1 illustrated a smaller drop in BET surface area (S_{BET}) and micropore volume (V_{micro}) of S-MCY, which suggested that the formation of mesopores was accompanied by partly detrimental effect on the micropore structure. The Hierarchy Factor (HF), defined as $(V_{mic} / V_{total}) \times (S_{Ext} / S_{BET})$, was cited to describe the hierarchical properties[26]. Obtained from data listed in table 1, higher HF value (HF = 0.149) of S-MCY were calculated than MCY (HF = 0.135). S-MCY primary nanocrystal size from BET area was 28.4 nm and decreased 7.2 nm comparing to MCY. So it can be concluded that small crystal size creates higher level of mesoporosity.

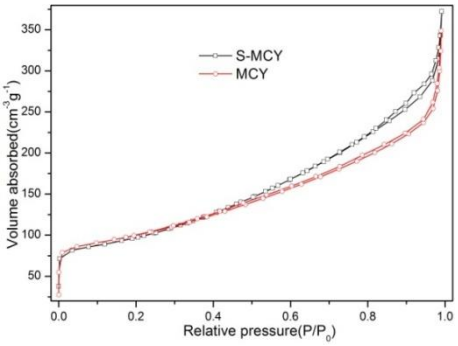

Fig. 4. N_2 adsorption - desorption isotherms for S-MCY and MCY.

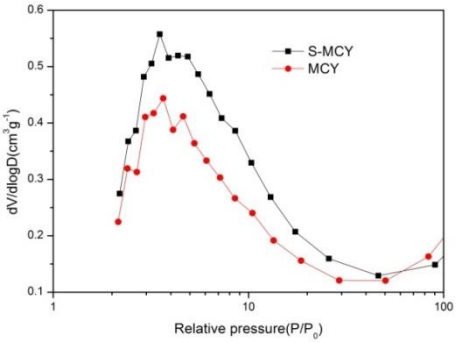

Fig. 5. BJH pores size distribution of zeolites.

Table 1. Textural parameters of catalysts.

Sample	S_{BET}[a] (m^2g^{-1})	S_{Ext} (m^2g^{-1})	S_{Micro}[b] (m^2g^{-1})	V_{Total}[c] ($cm^3\ g^{-1}$)	V_{Micro}[b] ($cm^3\ g^{-1}$)	V_{Meso}[d] ($cm^3\ g^{-1}$)	D_{Ext}[e] (nm)
S-MCY	333.1	143.2	189.9	0.576	0.148	0.428	28.4
MCY	334.7	114.1	220.6	0.540	0.153	0.387	35.6

a the total was obtained using the BET method; b the micropore surface area and micropore volume were obtained using the t-plot method; c the total pore volume is assumed to be the volume of adsorbed nitrogen at P/P_0 = 0.99; d mesopore volume was calculated by $(V_{total} - V_{micro})$; e obtained using the equation $D_{ext}=4061/S_{Ext}$.

The acid acidic properties of the catalysts are characterized by temperature programmed desorption using NH_3 as the probe molecule. As illustrated in Fig. 6, the desorption peaks located at 500 K and 623 K correspond to weak acid sites and strong acid sites respectively. The specific area is proportional to the amount of acid sites in the samples and can be calculated by the Gaussian curve-fitting [27] . The profiles showed that the area of S-MCY slightly smaller than the MCY. This was suggesting that the total acid amounts of S-MCY less than MCY. Through the Gaussian curve-fitting, S-MCY exhibited less both weak and strong acid sites, referring as MCY. Weak acid sites relied on H bonds and O-Si bonds, and strong acid sites related to the Al atoms. So, the loss of acid sites can be attributed to a lower proportion of framework Si and Al species [28]. This suggestions indicated the smaller crystal size of zeolite, the more defects introduced in the leaching treatment. More defects lead to a reduction in aluminium and silicon concentration of the S-MCY with small crystal structure, as well as the decreasing acidity amount.

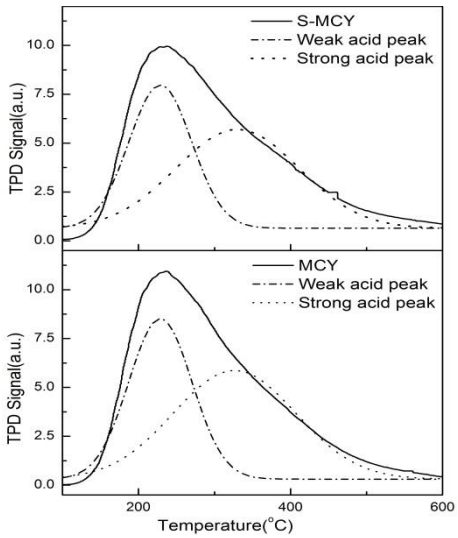

Fig. 6. NH_3-TPD profiles of S-MCY and MCY.

As presented in Fig. 7, from the catalytic performance on the MCY samples at 523K, TIPB conversion of 93.94 %, yield of cumene 6.27 wt%, yield of DIPB 44.06 wt% and propylene of 40.95 wt% were achieved. Compared to MCY, the catalyst S-MCY with small grain size exhibits a better catalytic cracking property. And a TIPB conversion of 96.43 %, yield of cumene 4.54 wt%, yield of DIPB 50.39 wt% and propylene of 43.54 wt% are presented. This result proved that catalyst S -MCY had a superior catalytic performance of TIPB, compared to MCY. As previous literatures reported [15, 20], the acidity and porous structure were two important factors in catalytic reaction. Usually, the main products of TIPB cracking are propylene, benzene, cumene, and diisopropylbenzene (DIPB) isomers. The kinetic diameter of TIPB, 1,3-DIPB, cumene, and benzene are 0.94, 0.84, 0.68 and 0.49 nm [29, 30]. DIPB isomers are regarded as TIPB pre-cracking products, and benzene and cumene are producted by deep cracking of TIPB molecules. Propylene is formed at each stage [31, 32]. As we all known, common zeolite Y possesses an aperture of micropores of 0.74 nm, which is smaller than kinetic diameter of TIPB. TIPB molecule is bulky enough and can be considered as a difficult-to-process feed. It is expected that the TIPB molecules are pre-cracked to produce DIPB isomers, which can diffuse into micropores. Following, DIPB isomers are cracked to cumene and benzene on the acid sites of the catalyst. So in pre-cracking process, the reaction activity is affected by both acidity and porous structure of catalyst. Mesopores facilitate the transport of reactant, and high acid amounts provided more active sites. The porous structure revealed that more mesopores were introduced in S-MCY catalyst rather than MCY catalyst (Table 1). But acidic sites of S-MCY catalyst preserved less than MCY (Table 2), suggesting that the textual structure of the catalysts play eventually a key role in pre-cracking stage. Due to the kinetic diameter of DIPB and cumene can diffuse into micropores.

So, in deep cracking process, the reaction activity was affected by only acidity of catalyst. Due to the less acidic sites of S-MCY, yield of cumene decreased.

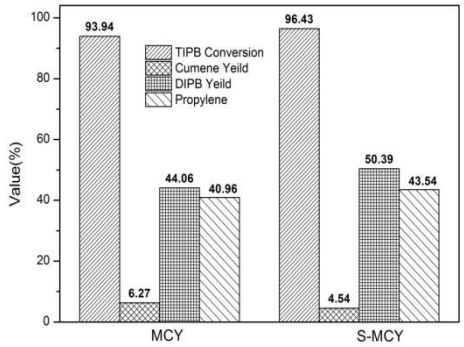

Fig. 7. Conversion of TIPB and product distribution on S-MCY and MCY samples at 523K.

4. Conclusions

Citric acid leaching and surfactants-assisted alkaline treatments in the presence of CTAB were used to obtain the mesoporous zeolite Y. The influence of small crystal size was investigated on S-MZY, referring to MZY. Results of texture properties showed that S-MCY sample exhibited larger mesopore volume and higher hierarchy factor, suggesting that the more mesopores were created. Small crystal size created higher level of mesoporosity. NH_3-TPD results showed that the total acid amounts of S-MCY less than MCY samples as well as strong/ weak acid amount. On the catalytic cracking performance of TIPB, S-MCY catalyst has higher catalytic activity and DIPB yield. It is mean that the textual structure of the catalysts plays eventually a key role in the process.

Acknowledgments

The authors acknowledge support from the Science and Technology Research Project of Colleges and Universities in Hebei Province (BJ2019203), Xingtai Young Talents Plan Project (2020ZZ040), Fundamental Research Funds for the Central Universities (3142019014).

References

[1] A. Corma, V. Fornés, J. Martínez-Triguero, S. B. Pergher, Journal of Catalysis **186**(1), 57 (1999).
[2] X. Zhao, X. Meng, Y. Shang, Y. Song, R. Liu, J. Wei, Y. Gong, Z. Li, Microporous and Mesoporous Materials **264**, 92 (2018).
[3] F. Tian, Q. Shen, Z. Fu, Y. Wu, C. Jia, Fuel Processing Technology **128**, 176 (2014).
[4] Q. Yu, H. Sun, H. Sun, L. Li, X. Zhu, S. Ren, Q. Guo, B. Shen, Microporous and Mesoporous Materials **273**, 297 (2019).
[5] L. Meng, X. Zhu, W. Wannapakdee, R. Pestman, M. G. Goesten, L. Gao, A. J. F. van Hoof, E. J. M. Hensen, Journal of Catalysis **361**, 135 (2018).
[6] O. S. Travkina, M. R. Agliullin, N. A. Filippova, A. N. Khazipova, I. G. Danilova, N. G. Grigor'Eva, N. Narender, M. L. Pavlov, B. I. Kutepov, RSC Advances **7**(52), 32581 (2017).
[7] A. Inayat, C. Schneider, W. Schwieger, Chemical Communications **51**(2), 279 (2015).
[8] J. R. García, M. Falco, U. Sedran, Catalysis Today **296**, 247 (2017).
[9] K. A. Cychosz, R. Guillet-Nicolas, J. Garcia-Martinez, M. Thommes, Chemical Society

Reviews **46**(2), 389 (2017).
[10] K. P. de Jong, J. Zečević, H. Friedrich, P. E. de Jongh, M. Bulut, S. van Donk, R. Kenmogne, A. Finiels, V. Hulea, F. Fajula, Angewandte Chemie International Edition **49**(52), 10074 (2010).
[11] J. García-Martínez, M. Johnson, J. Valla, K. Li, J. Y. Ying, Catalysis Science & Technology **2**(5), 987 (2012).
[12] J. G. Martinez, C. Xiao, K. A. Cychosz, K. Li, W. Wan, X. Zou, M. Thommes, Chem Cat Chem **6**(11), 3110 (2014).
[13] W. Q. Jiao, J. Ding, Z. B. Shi, X. M. Liang, Y. M. Wang, Y. H. Zhang, Y. Tang, M. He, Microporous and Mesoporous Materials **228**, 237 (2016).
[14] D. Reinoso, M. Adrover, M. Pedernera, Ultrasonics Sonochemistry **42**, 303 (2018).
[15] J. Shao, T. Fu, J. Chang, W. Wan, R. Qi, Z. Li, Journal of Fuel Chemistry and Technology **45**(1), 75 (2017).
[16] S. Mintova, M. Jaber, V. Valtchev, Chemical Society Reviews **44** (20), 7207 (2015).
[17] H. Awala, J. Gilson, R. Retoux, P. Boullay, J. Goupil, V. Valtchev, S. Mintova, Nature Materials **14**(4), 447 (2015).
[18] L. Tosheva, V. P. Valtchev, Chemistry of Materials **17**(10), 2494 (2005).
[19] C. H. L. Tempelman, X. Zhu, K. Gudun, B. Mezari, B. Shen, E. J. M. Hensen, Fuel Processing Technology **139**, 248 (2015).
[20] J. Zhao, Y. Yin, Y. Li, W. Chen, B. Liu, Chemical Engineering Journal **284**, 405 (2016).
[21] L. Hu, Z. Zhang, S. Xie, S. Liu, L. Xu, Catalysis Communications **10**(6), 900 (2009).
[22] W. Q. Jiao, W. H. Fu, X. M. Liang, Y. M. Wang, M. He, RSC Advances **4**(102), 58596 (2014).
[23] Z. Wang, H. Liu, Q. Meng, J. Jin, C. Xu, X. Mi, X. Gao, H. Liu, RSC Advances **7**(16), 965 (2017).
[24] E. Koohsaryan, M. Anbia, Materials Letters **236**, 390 (2019).
[25] S. Oruji, R. Khoshbin, R. Karimzadeh, Fuel Processing Technology **176**, 283 (2018).
[26] X. Zhang, D. Cheng, F. Chen, X. Zhan, Chemical Engineering Science **168**, 352 (2017).
[27] H. Sun, L. Sun, F. Li, L. Zhang, Fuel Processing Technology **134**, 284 (2015).
[28] N. Katada, Y. Kageyama, KazueTakahara, TakahideKanai, H. Begum, M. Niwa, Journal of Molecular Catalysis A: Chemical **211**(1-2), 119 (2004).
[29] S. Al-Khattaf, and H. de Lasa, Applied Catalysis A, General **226**(1), 139(2002).
[30] M. S. Aghakhani, A. A. Khodadadi, S. Najafi, Y. Mortazavi, Journal of Industrial and Engineering Chemistry **20**(5), 3037 (2014).
[31] Q. Jian, Z. Tianbo, X. Xin, L. Fengyan, S. Guida, China petroleum processing & petrochemical technology **12**(1), 17 (2010).
[32] N. Hosseinpour, Y. Mortazavi, A. Bazyari, A. A. Khodadadi, Fuel Processing Technology **90**(2), 171 (2009).